Journal of Solid State Chemistry 182 (2009) 1742–1748

Contents lists available at ScienceDirect

Journal of Solid State Chemistry

journal homepage: www.elsevier.com/locate/jssc

Influence of electrospraying parameters on the microstructure of $La_{0.6}Sr_{0.4}Co_{0.2}F_{0.8}O_{3-\delta}$ films for SOFCs

Daniel Marinha, Cécile Rossignol, Elisabeth Djurado *

Laboratoire d'Electrochimie et de Physico-Chimie des Matériaux et des Interfaces, 1130 rue de la Piscine, B.P. 75, 38402 St. Martin d'Hères, Grenoble Institute of Technology/UJF/CNRS (UMR5631), France

ARTICLE INFO

Article history:
Received 23 January 2009
Received in revised form
3 April 2009
Accepted 5 April 2009
Available online 24 April 2009

Keywords:
SOFC
$La_{0.6}Sr_{0.4}Co_{0.2}Fe_{0.8}O_{3-\delta}$
LSCF
Electrostatic spray deposition
ESD
$Ce_{0.9}Gd_{0.1}O_{2-\delta}$
CGO

ABSTRACT

Ceramics can play a remarkable role in the engineering of intermediate temperature solid oxide fuel cells (IT-SOFCs) capable of meeting the ambitious targets of reduced cost and improved lifetime. While mixed ionic–electronic conductors such as $La_xSr_{1-x}Co_yFe_{1-y}O_{3-\delta}$ are being used as volumic cathodes to increase the catalytic performance of these components, adequate microstructures are also an important requirement for optimal performance, particularly at lower operating temperatures. This work is devoted to the fabrication of $La_{0.6}Sr_{0.4}Co_{0.2}Fe_{0.8}O_{3-\delta}$ films on $Ce_{0.9}Gd_{0.1}O_{2-\delta}$ substrates by electrostatic spray deposition (ESD) and to the characterization of the microstructural dependence on the deposition conditions. A wide variety of microstructures ranging from dense to porous, with particular features such as reticulation and micro-porosity, were obtained by varying the ESD deposition parameters: nozzle-to-substrate distance (15, 30, 43, 45, and 58 mm), solution flow rate (0.34 and 1.5 mL/h), and substrate temperature (300, 350, 400 and 450 °C). The correlation between deposition parameters and resulting microstructures was systematically studied and put into evidence.

1. Introduction

The main goal of current research on solid oxide fuel cells is to improve the performance of solid oxide fuel cells operating at temperatures ranging from 500 to 700 °C. These so called IT-SOFCs are expected to increase useful lifespan and reduce operation costs, making them more practical and commercially more attractive. Unfortunately, detrimental phenomena such as electrolyte ohmic losses and cathode polarization increase at lower temperatures. To compensate for the efficiency reduction, alternative electrolyte and cathode materials are being evaluated as potential candidates for IT-SOFCs. $Ce_{0.9}Gd_{0.1}O_{2-\delta}$ (CGO) [1,2] is being studied as a replacement for conventional YSZ electrolytes due to its higher ionic conductivity values in the 500–700 °C range [3,4]. On the cathode side, $La_{1-x}Sr_xCo_{1-y}Fe_yO_{3-\delta}$ LSCF [5,6] has surfaced as a promising material due to its improved ionic conductivity relatively to LSM [7–9] and good chemical and physical compatibility with CGO [7,9]. These properties can be adjusted by changing the concentration of dopants [10–12], and a compromise between conductivity and mechanical compatibility with CGO can be attained for the $La_{0.6}Sr_{0.4}Co_{0.2}Fe_{0.8}O_{3-\delta}$ composition.

Microstructural design of the cathode film is also an important factor when considering optimal performances [13,14]. A combination of porous microstructures and small particle size enhances the catalytic properties by improving gas intrusion and enlarging the reactive surface areas. The possibility to produce different types of microstructures using the same synthesis technique would therefore be interesting for a systematic study correlating film morphology and electrochemical properties, while limiting the amount of variables, such as compositional differences.

Unlike other deposition techniques, electrostatic spray deposition (ESD) provides the possibility to obtain a wide range of very distinct microstructures in a fairly simple way. In this technique an aerosol is created and guided by an electrical field imposed on a metallic nozzle towards a grounded substrate which is normally heated. The shape and spraying modes of the aerosol may be tuned by changing the applied voltage [15]. The most stable configuration is known as the cone-jet mode and it can be obtained in a relatively small range of applied voltages for each set of experimental conditions [16]. The chemical composition of the aerosol is strictly determined by that of a precursor solution being pumped to the nozzle, granting control over the stoichiometry of the deposited layer. A large variety of microstructures can be tailored by varying the deposition parameters. The droplet size in the aerosol can vary from ~10 [17] to 100 μm [15], according to the setup. This parameter is fundamental to understand the formation mechanism of film microstructures and is dictated by a

* Corresponding author. Fax: +33 4 7682 6777.
E-mail address: Elisabeth.Djurado@lepmi.inpg.fr (E. Djurado).

0022-4596/$ - see front matter © 2009 Elsevier Inc. All rights reserved.
doi:10.1016/j.jssc.2009.04.018

combination of the chemical nature of the solution and the deposition parameters. Some studies have determined mathematical relationships that model the effect of these parameters on the resulting droplet size [16,18,19]. These studies aim to predict the droplet size that forms at the nozzle due to an electrohydrodynamic interaction. GananCalvo's [16] solution $d \sim (\rho\varepsilon_0 Q^3/\gamma K)^{1/6}$, which correlates droplet size d, with density ρ, vacuum permeability ε_0, flow rate Q, surface tension, γ and electrical conductivity K, of the solution, is possibly the most consensual in the literature.

A recent study from Wilhelm et al. [19] models the dynamic changes of the droplet size during its transport towards the substrate, starting from GananCalvo's model. A detailed review on the topic has been reported by Jaworeck [15]. Ultimately, the morphological features of the deposited layer are determined by the size of the droplet and its interaction with the heated substrate (impact, spreading, drying and precursor decomposition).

In conclusion, ESD is a fast and easy way to deposit pure, composite or graded oxide layers. It is less expensive than other deposition techniques, which typically require vacuum, and it is also highly flexible, allowing for a large selection of materials to be deposited. Previous studies in our laboratory have successfully used ESD to deposit YSZ [20] and LSM/YSZ composite layers [21]. Elsewhere, ESD has also been used to deposit different compositions of the LSCF family on glass and stainless steel [11,22]. This technique has also been used to deposit LSCF on CGO substrates but only one microstructure was reported [22]. This paper reports a systematic study of the influence of nozzle-to-substrate distance, solution flow rate and substrate temperature on the microstructure of $La_{0.6}Sr_{0.4}Co_{0.2}Fe_{0.8}O_{3-\delta}$ deposited over $Ce_{0.9}Gd_{0.1}O_{2-\delta}$ substrates for the first time. A correlation between these parameters and the resulting microstructures will be presented and discussed.

2. Experimental section

CGO substrates were prepared in the shape of disks, 19 mm in diameter and 1 mm thick. Powders (Praxair, 99.9%) were isostatically pressed at 250 MPa for 5 min and sintered at 1450 °C for 4 h in air. The surfaces of the densified pellets were machined to become parallel and then polished to guarantee uniform surface conditions.

Precursor salts solution was prepared by weighing $La(NO_3)_3.6H_2O$ (Prolabo, 99.99%), $SrCl_2.6H_2O$ (Strem Chemicals, 99%), $Co(NO_3)_2.6H_2O$ (Sigma-Aldrich, 99.999%) and $Fe(NO_3)_2.9H_2O$ (Sigma-Aldrich, 99.99%) salts in adequate amounts as to obtain the $La_{0.6}Sr_{0.4}Co_{0.2}Fe_{0.8}O_{3-\delta}$ stoichiometry. These were mixed in ethanol (C_2H_5OH, 99.9%; Prolabo) and diethylene glycol monobutyl ether, also known as butyl carbitol ($CH_3(CH_2)_3OCH_2$-$CH_2OCH_2CH_2OH$, 99+%; Acros Organics 99+%) with a 1:2 volume ratio and a total salt concentration of 0.02 mol/L.

The LSCF films were deposited using a vertical ESD setup (Fig. 1).

Depositions were made at different nozzle-to-substrate distances (15, 30, 43, 45 and 58 mm), and solution flow rates of 0.34 and 1.5 mL/h using a Sage™ M361 syringe pump. Deposition temperatures were of 300, 350, 400 and 450 °C. These values refer to the surface of the substrate facing the solution spray, and were obtained after temperature calibration. A positive high voltage was selected and applied between the nozzle and the hot plate, in order to generate the aerosol and the cone-jet spraying mode in each deposition. Values ranged from 5 to 12 KV. Bevelled stainless steel nozzles, 3 mm long and 0.6 mm in diameter, were used for spraying. Total deposition time remained fixed at 1 h.

Thermal decomposition of iron and cobalt nitrates, as well as of the precursor salt solution, were performed in air, from room temperature to 690 °C at a 10 °C/min heating rate, using a Netzsch simultaneous thermal analyzer STA 409 instrument. Microstructures and elemental analysis of the deposited films were studied using scanning electron microscopy (LEO S440) coupled with EDS detector (EDAX). X-ray powder diffraction was carried out on

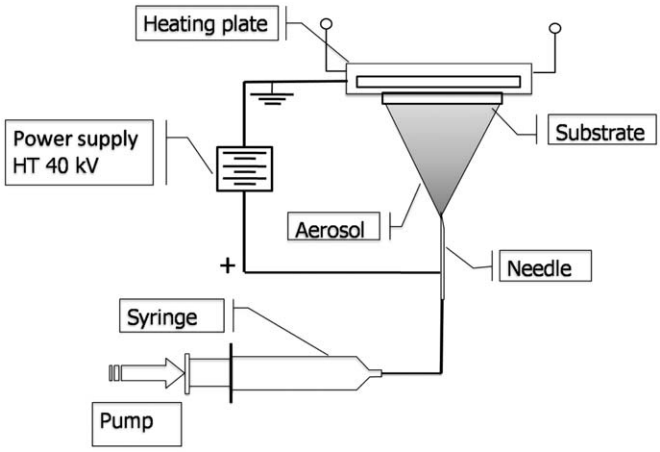

Fig. 1. Schematic drawing of the ESD setup used in sample preparation.

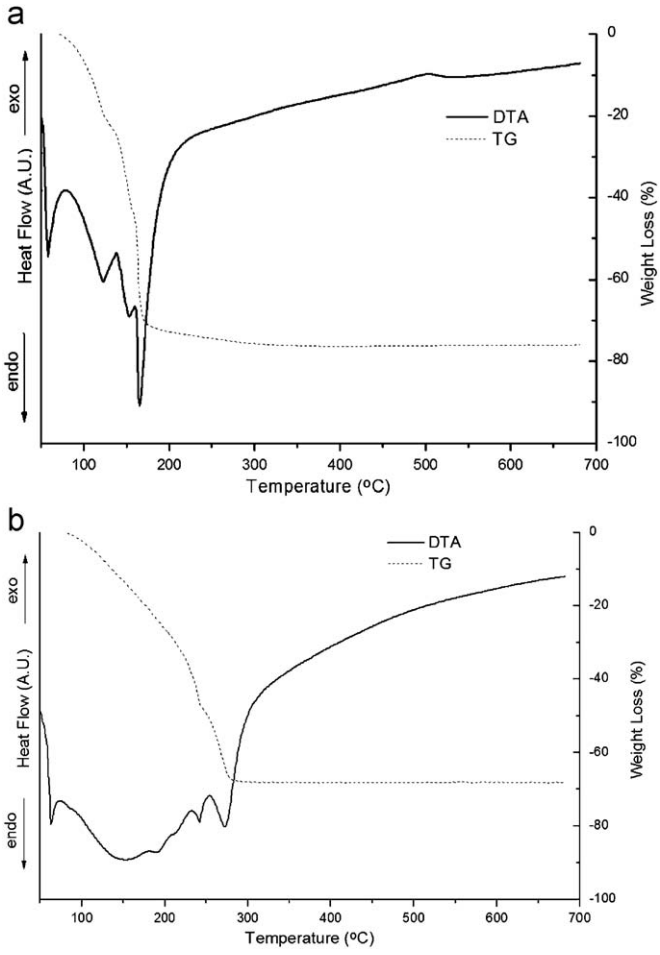

Fig. 2. TG/DTA plots of $Fe(NO_3)_2 \cdot 9H_2O$ (a) and $Co(NO_3)_2 \cdot 6H_2O$ (b) obtained at 10 °C/min in air.

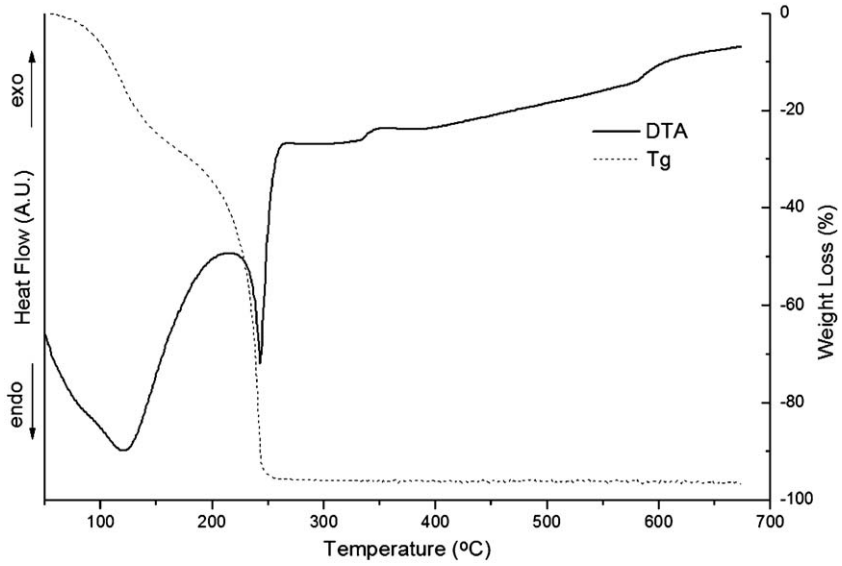

Fig. 3. DTA/TG plots of the LSCF precursor salt solution, obtained at 10 °C/min in air.

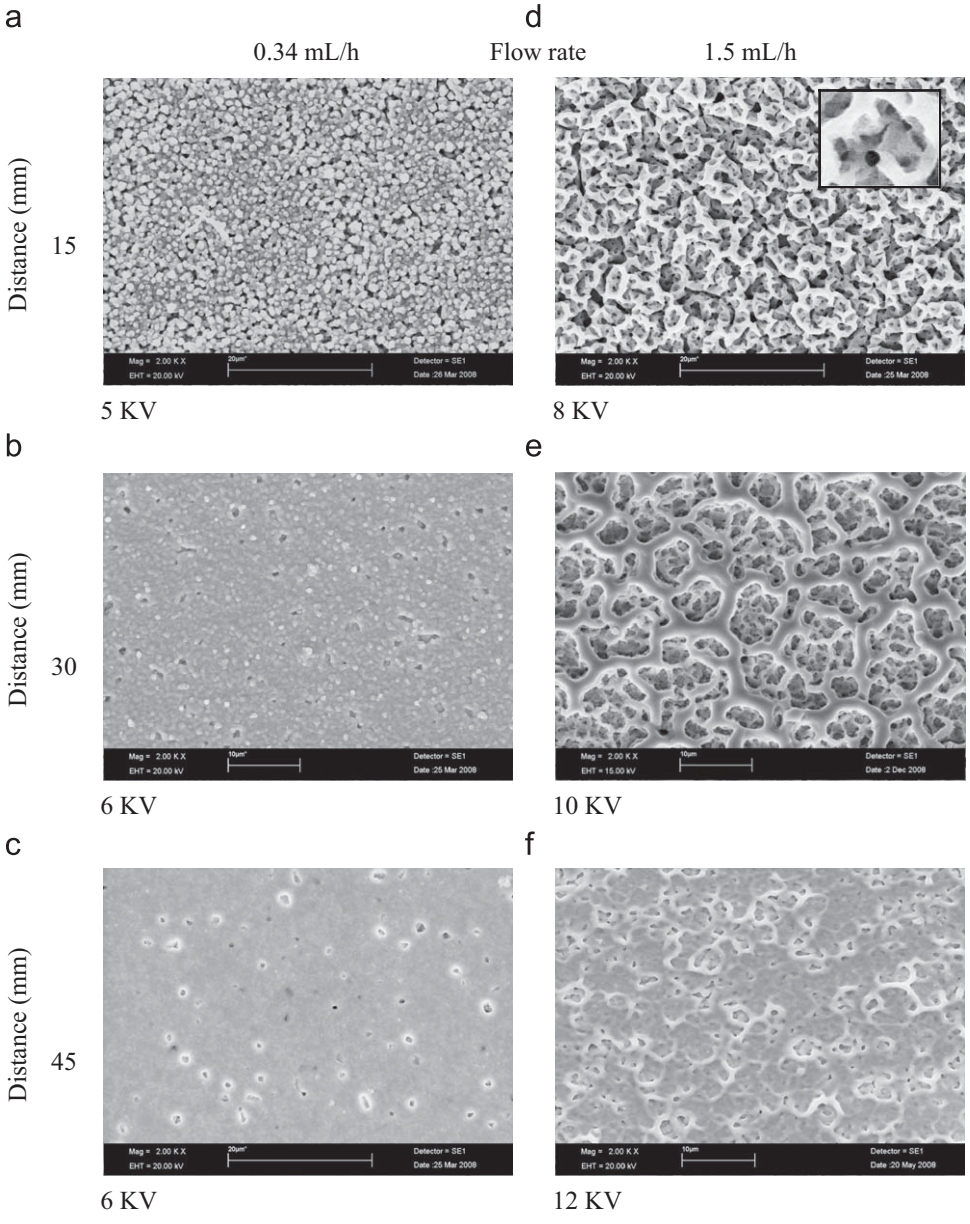

Fig. 4. SEM micrographs of $La_{0.6}Sr_{0.4}Co_{0.2}Fe_{0.8}O_{3-\delta}$ films deposited on CGO substrates at 300 °C for 1 h with gradually increasing distances for two different solution flow rates of 0.34 (left column) and 1.5 mL/h (right column). Applied voltage is indicated below each picture in Kilovolts. Inset: detail of an isolated pore.

samples post-annealed at 500, 700 and 900 °C for 2 h in air using a PANalytical X'Pert Pro MPD diffractometer in the Bragg–Brentano geometry from 20° to 120° in 2θ (0.017° in 2θ step, 30.5 s as a counting time) with Cu radiation. Phases were identified using EVA software.

3. Results and discussion

Preliminary studies were based on performing thermogravimetric and differential thermal analysis (TG/DTA) of iron and cobalt nitrates and of the precursor salts solution. The decomposition temperatures of the iron and cobalt nitrates occurred at 165 (Fig. 2a) and 274 °C (Fig. 2b), respectively. Previous TG/DTA analysis had shown that strontium chloride decomposes at 220 °C, whereas lanthanum nitrate has the highest decomposition temperature at 700 °C [23]. DTA/TG of the LSCF precursor solution (Fig. 3) shows two main endothermic peaks at 121 and 245 °C corresponding to the total evaporation of ethanol and butyl carbitol, respectively. Therefore, to induce formation of porosity on the films, the deposition temperature must be higher than that of the solvent evaporation.

Influence of nozzle-to-substrate distance. To study the effect of spraying distance on the morphology of the LSCF films, depositions were carried out at nozzle-to-substrate distances of 15, 30 and 45 mm and solution flow rates of 0.34 and 1.5 mL/h. Substrate temperature and total deposition time remained constant at 300 °C and 1 h, respectively. Resulting micrographs and experimental conditions were compiled and are presented in Fig. 4.

Microstructures of films deposited using a low solution flow rate of 0.34 mL/h (Fig. 4a–c) are composed of round-shaped particles that have successively coalesced on the substrate, creating a homogeneously porous layer.

As nozzle-to-substrate distance increases, deposited particles become increasingly smaller due to larger solvent losses through evaporation occurring during droplet flight as a result of the temperature gradient generated between the surface of the substrate and the nozzle. In a chain of events, the larger the distance, the longer it takes for the droplet to reach the substrate, allowing for greater solvent evaporation and resulting in drier droplets at the moment of impact with the substrate. Drier droplets are relatively smaller and so the deposited particles will also be smaller, leading to better packing and increase in film density. This can be observed for samples deposited at 30 and 45 mm in Fig. 4b and c. The gaps seen in the films can be attributed to the fact that the smaller particles do not create a layer thick enough to completely cover the porosity of the substrate, possibly caused by grain detachment during polishing (Fig. 5).

Films deposited using a solution flow rate of 1.5 mL/h (Fig. 4d–f) share the same general tendency previously discussed, resulting in denser microstructures at increasing distance values. At 15 mm the microstructure can be described as an irregular and porous network of LSCF, with sub-micron sized pores inside of the solid network (see inset in Fig. 4d). Regular reticulation of the LSCF occurs at 30 mm as the pores become laterally isolated, while remaining interconnected in a direction perpendicular to the surface of the substrate. According to Princivalle et al. [24], reticulation occurs due to simultaneous boiling and drying of the droplets on the surface of the substrate, when the temperature of the substrate is close to that of the boiling temperature of the solvents, which is consistent with our results. However, reticulation is also related with the droplet size, because it does not occur in all depositions performed at a given temperature. Fig. 6 depicts the initial stages of a droplet spreading along a flat and smooth surface [25]. If the droplet is relatively dry upon impact, then little

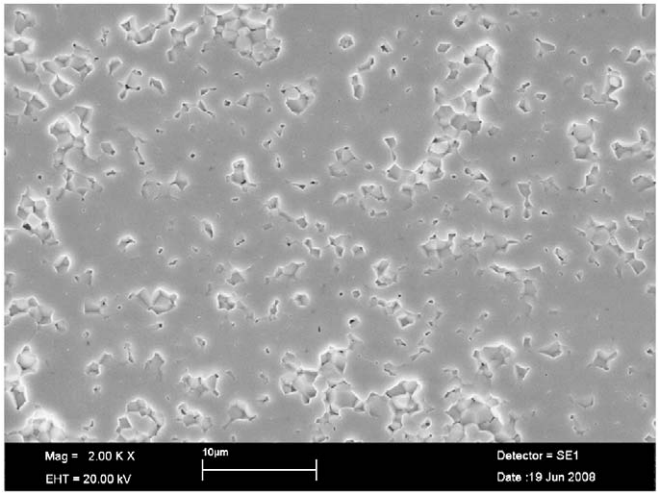

Fig. 5. Micrograph of the surface of a CGO substrate used in ESD depositions.

spreading will occur and the final microstructure will be similar to that of Fig. 4a, corresponding to stage (a) in Fig. 6. On the other hand, if the droplet retains enough solvent, the impact force causes it to spread on the surface before drying up and solidifying in any of the given configurations from Fig. 6a to h, according to drying and/or boiling rates. Therefore, reticulation requires the droplet to retain enough liquid upon impact and can be associated to solidification in stage (f).

The solid network in Fig. 4(d and e) is slightly cracked, most likely because of the high liquid content in the droplets upon impact. At this stage, cracks may appear as a result of the stresses generated by shrinkage of the layer during liquid evaporation and consequential drying of the film. At 45 mm (Fig. 4f), although some reticulation is still visible, it is almost completely hindered because droplets must cross larger distances and will be relatively drier upon arrival, creating a denser and crack-free layer.

Influence of precursor solution flow rate. According to Ganan-Calvo's relationship, larger droplets are generated at the tip of the nozzle when the solution flow rate is increased. This can be empirically confirmed by comparing the morphology of the films deposited at different flow rates. As larger droplets imply a greater amount of liquid, they can endure longer flight times without drying up completely. Comparison between the micrographs of each column in Fig. 4 shows that raising the solution flow rate induces different types of reticulation of the microstructure. The degree and type of reticulation varies (Fig. 4d–f) and depends on a combination of both distance and flow rate, which is logical because both have an effect on the size of the droplet at the moment of impact with the substrate. However, flow rate has a more direct role on the size of the droplet created at the outcome of the nozzle, whereas distance influences the size of the droplet upon impact by providing more or less time for drying to occur during its flight. This implies that flow rate imposes an *a priori* limit to the maximum droplet size, whereas distance can be used to control the minimum droplet size at the moment of impact. This is important because even though both parameters have similar effects on droplet size in certain regimes, different practical consequences may still arise from each. For example, if given enough distance, the droplets will dry up completely giving rise to completely different microstructures due to preferential landing effects, as will be seen next.

Influence of deposition temperature. Fig. 7 shows the morphological evolution of the films deposited at different temperatures (300, 350, 400 and 450 °C) and at two different distances (43 and 58 mm). Solution flow rate and deposition time

were maintained fixed at 1.5 mL/h and 1 h, respectively. As previously discussed, reticulation occurs for a substrate temperature of 300 °C and a relatively high flow rate of 1.5 mL/h. No film reticulation is observed at depositions made at a temperature of 350 °C and higher because this increases the solvent evaporation rate, resulting in drier and smaller droplets.

By further increasing deposition temperature, a point is reached when the droplets dry completely during flight and reach the substrate as solidified particles. Under such conditions, these particles tend to overlap during deposition, rather than spreading homogeneously along the substrate. This is known as preferential landing effect and occurs due to the electrostatic attraction between the charged particles of the spray and surface points with higher curvatures. It becomes more pronounced at higher temperatures and larger distances because the smaller the particles are, the easier they are diverted. Fig. 7c–f are examples of this effect.

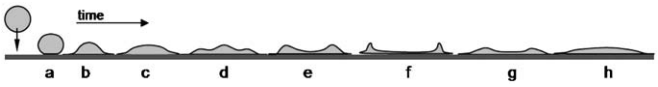

Fig. 6. Initial stages of a liquid droplet spreading on a flat, smooth surface [25].

This set of images shows that deposition temperature and nozzle-to-substrate distance influence droplet size in different ways. Although temperature influences the evaporation rate, distance determines the available drying time. Different consequences arise from this fact. Distance also allows more or less time for the particles to alter their trajectories due to preferential landing effect. Indeed, a larger distance leads to smaller particles to be deposited, as shown in Fig. 7d–f deposited at 58 mm, with comparison to Fig. 7a–c deposited at 43 mm.

Temperature plays a similar role by conditioning the drying rate of the droplets during flight, but will also determine the rate at which they dry once they deposit on the substrate and also, to some extension, the way in which droplets spread on its surface

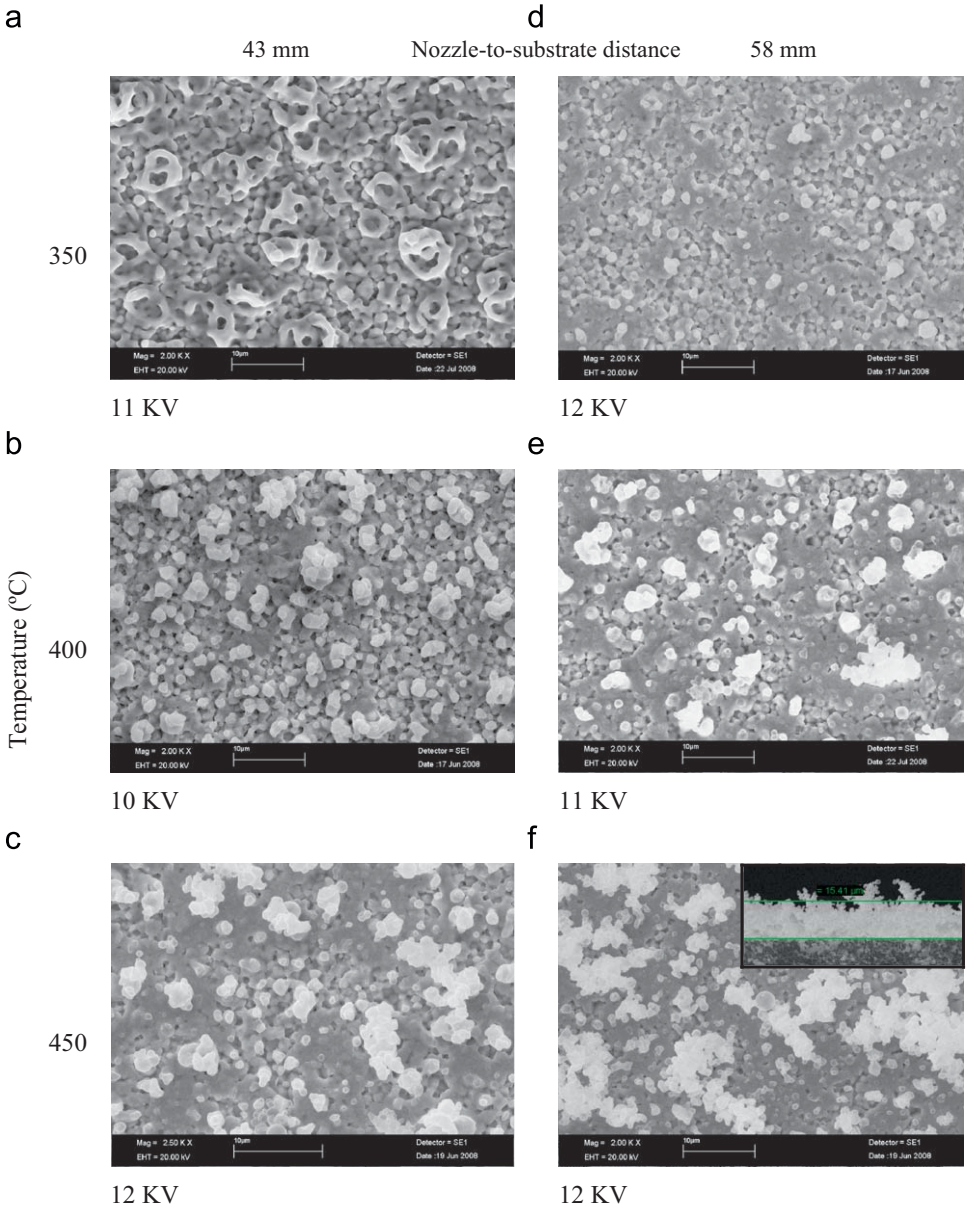

Fig. 7. SEM micrographs of $La_{0.6}Sr_{0.4}Co_{0.2}Fe_{0.8}O_{3-\delta}$ films deposited on CGO substrates using a constant solution flow rate of 1.5 mL/h for 1 h and at increasing temperature for two different nozzle-to-substrate distances of 43 mm (left column) and 58 mm (right column). Applied voltage is indicated below each picture in kilovolts. Inset: cross section view of the LSCF film.

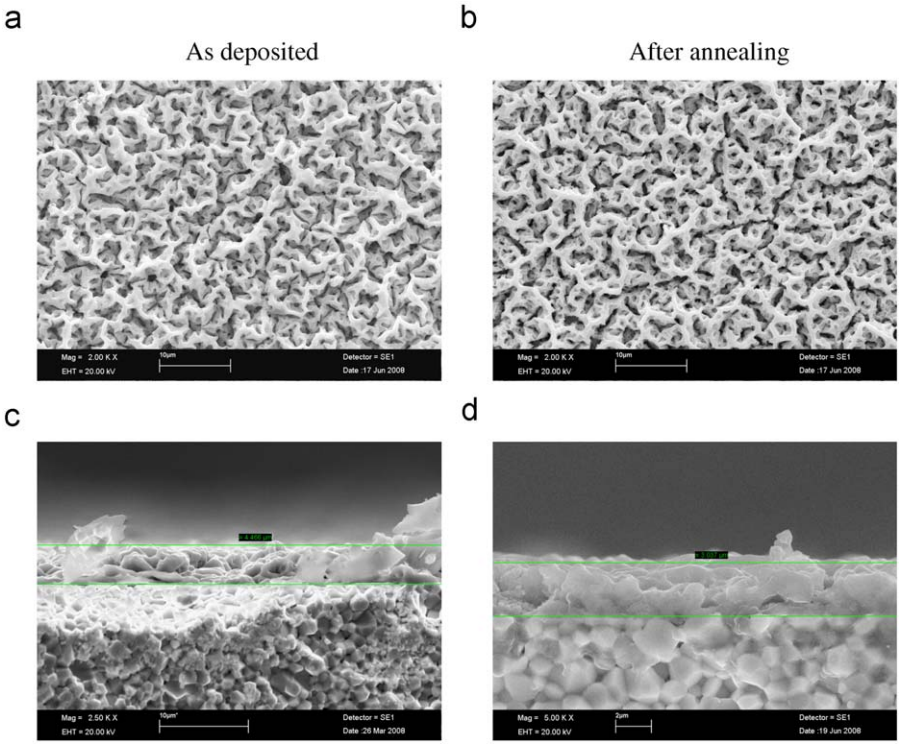

Fig. 8. SEM micrographs of the surface of the film, (a) and (b), and of its cross-section, (c) and (d), taken before and after sample annealing at 900 °C.

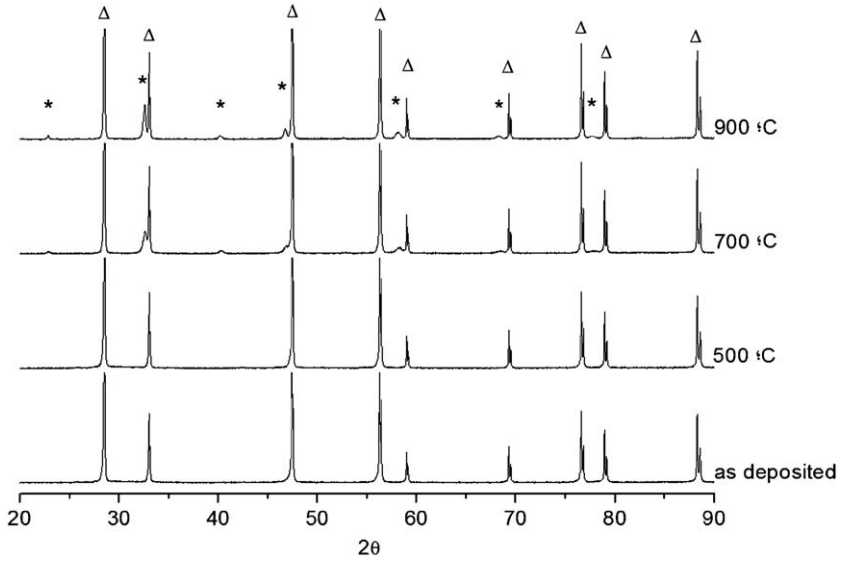

Fig. 9. XRD patterns of LSCF (*) and CGO (Δ) phases obtained at different annealing temperatures with LSCF crystallization occurring between 500 and 700 °C.

and, ultimately, the resulting microstructure. It is visible in these microstructures that a superficial layer of LSCF film is previously created before these structures begin to appear. This is consistent with the phenomenon of preferential landing effect which requires that some particles randomly deposit near each other to create points on the substrate with higher curvatures, on top of which following particles successfully accumulate.

Heat treatment. The influence of heat treatment on film morphology and thickness was studied on a sample deposited using a flow rate of 1.5 mL/h, nozzle-to-substrate distance of 15 mm and substrate temperature of 300 °C for 1 h, and on the crystallization of the film.

SEM micrographs taken before and after annealing (Fig. 8) show that heat treatment in air at 900 °C for 2 h, caused a slight decrease in film thickness from ~4 to ~3 μm due to film densification and the departure of organic residues, while no visible alterations occurred to its morphology.

This is an important result for the application of such films as cathodes on IT-SOFCs operating at 700 °C for long periods of time. EDS performed on the surface of the samples consistently detected the presence of La, Sr, Co and Fe from the film, as well as Ce and Gd which correspond to the elemental composition of the substrate. Good adhesion between the film and the substrate was verified in a scotch test. X-ray

diffraction performed after successive heat treatments at 500, 700 and 900 °C shows that as-deposited films are amorphous and that crystallization occurs between 500 and 700 °C in the perovskite structure (Fig. 9). No impurity or secondary phases were detected.

4. Conclusions

A systematic study of the influence of deposition parameters on the microstructure of LSCF films deposited by ESD on CGO substrates has been presented. ESD was established as a valid and interesting technique to deposit $La_{0.6}Sr_{0.4}Co_{0.2}Fe_{0.8}O_{3-\delta}$ films on CGO substrates with potential advantages in microstructural design of IT-SOFCs cathode films.

It was shown how ESD allows for wide variety of morphological variations to be obtained by altering the nozzle-to-substrate distance, solution flow rate and substrate temperature. A correlation between deposition parameters, droplet size and microstructural features of resulting films were discussed. The correlation between the studied parameters and droplet size is significantly different at different stages of the deposition: flow rate determines the initial droplet size; nozzle-to-substrate distance and temperature determine the dynamic change of the droplet size during flight; and the latter ultimately influences spreading and drying of the droplets on the substrate. The microstructure of the deposited layer will therefore be the result of the interaction between droplets with a given liquid content and the combined effects of spreading and drying rates determined by the substrate temperature at the moment of impact.

The possibility of creating and controlling different aspects of film morphology such as solid material and porosity arrangements is of great interest to IT-SOFCs technology, and opens the door for posterior electrochemical studies to understand how these affect the overall performance of the fuel cells.

References

[1] B.C.H. Steele, Solid State Ionics 129 (2000) 95–110.
[2] K.R. Reddy, K. Karan, J. Electroceram. 15 (2005) 45–56.
[3] H.L. Tuller, A.S. Nowick, J. Electrochem. Soc. 122 (1975) 255–259.
[4] M. Sahibzada, B.C.H. Steele, K. Zheng, R.A. Rudkin, I.S. Metcalfe, Catal. Today 38 (1997) 459–466.
[5] D. Beckel, A. Dubach, A.R. Studart, L.J. Gauckler, J. Electroceram. 16 (2006) 221–228.
[6] F. Tietz, Q. Fu, V.A.C. Haanappel, A. Mai, N.H. Menzler, S. Uhlenbruck, Int. J. Appl. Ceram. Technol. 4 (2007) 436–445.
[7] A. Esquirol, N.P. Brandon, J.A. Kilner, M. Mogensen, J. Electrochem. Soc. 151 (2004) A1847–A1855.
[8] L.W. Tai, M.M. Nasrallah, H.U. Anderson, D.M. Sparlin, S.R. Sehlin, Solid State Ionics 76 (1995) 273–283.
[9] L.W. Tai, M.M. Nasrallah, H.U. Anderson, D.M. Sparlin, S.R. Sehlin, Solid State Ionics 76 (1995) 259–271.
[10] L. Qiu, T. Ichikawa, A. Hirano, N. Imanishi, Y. Takeda, Solid State Ionics 158 (2003) 55–65.
[11] C.Y. Fu, C.L. Chang, C.S. Hsu, B.H. Hwang, Mater. Chem. Phys. 91 (2005) 28–35.
[12] S.R. Wang, T. Kato, S. Nagata, T. Honda, T. Kaneko, N. Iwashita, M. Dokiya, Solid State Ionics 146 (2002) 203–210.
[13] J. VanHerle, A.J. McEvoy, K.R. Thampi, Electrochim. Acta 41 (1996) 1447–1454.
[14] P. Holtappels, C. Bagger, J. Eur. Ceram. Soc. 22 (2002) 41–48.
[15] A. Jaworek, A.T. Sobczyk, J. Electrostat. 66 (2008) 197–219.
[16] A.M. GananCalvo, J. Davila, A. Barrero, J. Aerosol Sci. 28 (1997) 249–275.
[17] O. Wilhelm, S.E. Pratsinis, D. Perednis, L.J. Gauckler, Thin Solid Films 479 (2005) 121–129.
[18] J.F. Delamora, I.G. Loscertales, J. Fluid Mech. 260 (1994) 155–184.
[19] O. Wilhelm, L. Madler, S.E. Pratsinis, J. Aerosol Sci. 34 (2003) 815–836.
[20] T. Nguyen, E. Djurado, Solid State Ionics 138 (2001) 191–197.
[21] A. Princivalle, D. Perednis, R. Neagu, E. Djurado, Chem. Mater. 17 (2005) 1220–1227.
[22] I. Taniguchi, R.C. van Landschoot, J. Schoonman, Solid State Ionics 156 (2003) 1–13.
[23] A. Princivalle, D. Perednis, R. Neagu, E. Djurado, Chem. Mater. 16 (2004) 3733–3739.
[24] A. Princivalle, E. Djurado, Solid State Ionics 179 (2008) 1921–1928.
[25] R. Neagu, D. Perednis, A.S. Princivalle, E. Djurado, Chem. Mater. 17 (2005) 902–910.